Journal of Volcanology and Geothermal Research 440 (2023) 107857

Contents lists available at ScienceDirect

Journal of Volcanology and Geothermal Research

journal homepage: www.journals.elsevier.com/journal-of-volcanology-and-geothermal-research

Silicic frothy xenoliths (xeno-pumice) in recent volcanics from Gran Canaria, Canary Islands

S.B. Jägerup [a,b,*], V.R. Troll [a,c,*], H. Geiger [a,d], F.M. Deegan [a], C. Harris [e], J.C. Carracedo [c], F.C. Meade [a], S. Omidian [a], K. Zaczek [a], F.M. van der Zwan [b]

[a] Department of Earth Sciences, Natural Resources and Sustainable Development (NRHU), Uppsala University, Uppsala, Sweden
[b] Faculty of Physical Science and Engineering, King Abdullah University of Science and Technology (KAUST), Thuwal, Saudi Arabia
[c] Department of Physics (GEOVOL), University of Las Palmas de Gran Canaria (ULPGC), Las Palmas de Gran Canaria, Canary Islands, Spain
[d] Institute of Earth and Environmental Sciences, University of Freiburg, Freiburg im Breisgau 79104, Germany
[e] Department of Geological Sciences, University of Cape Town, Rondebosch 7701, South Africa

ARTICLE INFO

Keywords:
Gran Canaria
Alkaline volcanism
Xenoliths
Xeno-pumice
Magma-sediment interaction

ABSTRACT

The Quaternary small-volume alkaline magmatic episode on Gran Canaria erupted dominantly basanite and nephelinite lavas and scoria deposits that contain a range of mantle and crustal xenoliths. These xenoliths comprise peridotite nodules, partially melted plutonic and volcanic rock fragments, and a group of light colored, felsic, and commonly frothy quartz-bearing rock fragments (xeno-pumice) that show evidence for intense interaction with their host magmas. Here we study a selection of these felsic and, in part, glassy and vesicular xenoliths from North and North-East Gran Canaria, with the aim to unravel their ultimate origin and learn more about magma storage and ascent within and below the island. Inspection of textures, mineral assemblages and glass compositions reveal one group of felsic xenoliths with fresh to partly altered igneous phenocryst assemblages and relict magmatic textures in addition to $\delta^{18}O$ values of 3.6 to 6.6‰. This group is interpreted to be of igneous origin. A second group of frothy felsic xenoliths displays mineralogy and textural characteristics more similar to sedimentary rocks with frequent occurrence of quartz, a mineral usually not present as phenocrysts in magmatic rocks from the Canary Islands. This second group displays relatively high $\delta^{18}O$ values (8.1 to 16.8‰), more typical for sedimentary lithologies, and is thus interpreted to represent material derived from the extensive pre-island sedimentary part of the ocean crust. The investigated xenoliths from North Gran Canaria thus provide a snapshot of pre-island sedimentary geology as well as the island's "magmatic" interior. These new data help constrain the available subsurface compositional variations within and below the Canary Islands and will hence be useful in interpreting magma evolution trends and magma storage levels.

1. Introduction

Magma is one of the most important probes into the Earth's interior and can provide information on magmatic sources, as well as on the rocks a magma has passed *en route* to the surface (e.g., Jolis et al., 2015; Bindeman et al., 2022; Day et al., 2022). In addition to the magma compositions, another crucial aspect in this respect are foreign rock fragments and inclusions (xenoliths) entrained in ascending magmas (e.g., Hansteen and Troll, 2003; Troll et al., 2012). Xenoliths can provide information on ascent and storage conditions of the host magma as well as on the nature and composition of the subvolcanic basement. In ocean islands, xenoliths may be derived from mantle depths (e.g., mantle nodules), the lower (magmatic) to upper (sedimentary) oceanic crust, or from the volcanic edifice itself (e.g., Rothe and Schmincke, 1968; Hoernle, 1998; Klügel, 1998; Schmincke et al., 1998; Neumann et al., 2002; Hansteen and Troll, 2003; Aparicio et al., 2006; Aparicio et al., 2010; Troll et al., 2012; Zaczek et al., 2015; Troll et al., 2015; Berg et al., 2016).

The most recent (Holocene) volcanic episode on Gran Canaria is characterized by mafic alkaline magmas that erupted tephra deposits, lava flows and, when in contact with near-surface water, phreatomagmatic tuff deposits from a series of cinder cones and maar volcanoes (Hoernle and Schmincke, 1993; Rodriguez-Gonzalez et al., 2009; Schmincke and Sumita, 2010; Aulinas et al., 2010a, 2010b). These

* Corresponding authors at: Department of Earth Sciences, Natural Resources and Sustainable Development (NRHU), Uppsala University, Uppsala, Sweden.
E-mail addresses: signebeatrice.jagerup@kaust.edu.sa (S.B. Jägerup), valentin.troll@geo.uu.se (V.R. Troll).

https://doi.org/10.1016/j.jvolgeores.2023.107857
Received 6 April 2023; Received in revised form 20 June 2023; Accepted 30 June 2023
Available online 3 July 2023

recent eruptive products on Gran Canaria contain, amongst other types of xenoliths, a small percentage of massive to pumice-textured felsic xenoliths that bear resemblance to either sedimentary, plutonic or volcanic rocks from the island's edifice. Some of these xenoliths were previously interpreted as frothed-up oceanic crust fragments (see Hoernle, 1998; Hansteen and Troll, 2003), and they resemble the frothy high-silica "xeno-pumice" (also locally known as "restingolites") that erupted near El Hierro in 2011 (e.g., Troll et al., 2012; Carracedo et al., 2015; Berg et al., 2016). However, the primary lithology for these frothy xenoliths at El Hierro was subject of intense debate. During the volcanic crisis of El Hierro in 2011, the xeno-pumice samples were considered by different workers as either vesiculated sedimentary rock, entrained felsic magma, or recycled hydrothermal rock from the volcanic edifice present in the upper crust (e.g. Troll et al., 2012; Meletlidis et al., 2012; Del Moro et al., 2015; Rodriguez-Losada et al., 2015). This uncertainty led the authorities at the time to consider the possibility of explosive felsic eruptions and to order repeated evacuations of the town of La Restinga at the southern tip of El Hierro Island (see Carracedo et al., 2015 for discussion). Only years after the eruption did the final origin of the El Hierro xeno-pumice samples get resolved, which was due to the recovery of nannofossils from the El Hierro xeno-pumice samples (Zaczek et al., 2015; Troll et al., 2015), defining them as melted and frothed up sedimentary materials from the pre-island ocean crust. Similar xeno-pumice samples have been described from several other Canary eruptions, such as the 1730–36 Timanfaya eruption on Lanzarote, the 1971 Teneguia eruption on La Palma, and from recent eruptions in the north of Gran Canaria (e.g. Rothe and Schmincke, 1968; Araña and Ibarrola, 1973; Hansteen and Troll, 2003; Aparicio et al., 2006, 2010, Carracedo et al., 2015; Carracedo and Troll, 2016). For example, pumiceous, acidic rocks from the 1971 eruption on La Palma were suggested by Araña and Ibarrola (1973) to represent bimodal mixing of rhyolitic and basaltic melt, while Aparicio et al. (2006) and Aparicio et al. (2010) described frothed up xenoliths from Lanzarote as meta-sedimentry lithologies. Given the uncertainties that exist, and the implications for hazard mitigation and civil protection responses to the occurrence of such xenoliths in the 2011 El Hierro eruption, a need for further investigation of this type of xenolith exists.

Here we report on a newly collected suite of felsic xenoliths within young eruptives from North and Northeast Gran Canaria that record a transition from massive to pumiceous textures, which thus allows a better understanding of the formation processes that give rise to 'xeno-pumice' in Canary eruptions. We aim to test the existing hypotheses on the composition and origin of Canary 'xeno-pumice' in regards to whether they represent remobilised rhyolitic magma or rocks, hydrothermally altered intra-edifice compositions, or high-silica sedimentary rocks that were exposed to heating and degassing while entrained in ascending magma (cf. Rothe and Schmincke, 1968; Hansteen and Troll, 2003; Aparicio et al., 2010; Meletlidis et al., 2012; Troll et al., 2012, 2015; Sigmarsson et al., 2013; Rodriguez-Losada et al., 2015; Carracedo et al., 2015; Zaczek et al., 2015; Berg et al., 2016). Through our study of the various textural and chemical xeno-pumice types from Gran Canaria, we now offer criteria on how to distinguish between different xeno-pumice types in a practical way, which will be of use for monitoring teams on the ground during future eruptions in the Canary Islands.

1.1. Geological setting

The Canary Islands are located in the Eastern Central Atlantic Ocean and comprise seven larger and several smaller volcanic islands. They stretch from about 100 to 500 km off the northwestern coast of Africa and are situated on top of the slow-moving Jurassic-aged oceanic plate (Morgan, 1971; Hoernle and Schmincke, 1993; Carracedo et al., 1998; Hoernle, 1998; Schmincke et al., 1998; Schmincke and Sumita, 2010; Carracedo and Troll, 2016, 2021). The details of their origin have been debated over the past five decades, but most authors favor a hot spot or plume-type model for their origin at present, although other concepts, such as a possible fracture control or small scale upper mantle convection next to the African continent, have also been discussed (Anguita and Hernán, 1975; Anguita and Hernan, 2000; Schmincke, 1982; Hoernle and Schmincke, 1993; King and Ritsema, 2000; Montelli et al., 2004; Carracedo et al., 1998, 2015; Zaczek et al., 2015; Carracedo and Troll, 2016, 2021). Gran Canaria is the central island of the archipelago (Fig. 1), and is ~45 km in diameter and 1939 m above sea level in maximum altitude (Krastel and Schmincke, 2002; Schmincke and Sumita, 2010). The island itself rests on thickened Jurassic ocean crust that is overlain by a ca. 2 km thick layer of Mesozoic to Miocene pre-island sedimentary strata (Hoernle, 1998; Schmincke et al., 1998; Ye et al., 1999; Krastel and Schmincke, 2002; Hansteen and Troll, 2003; Carracedo and Troll, 2016). These sedimentary deposits derive dominantly from continental Africa via aeolian and fluvial transport and experience marine sedimentary reworking via for example turbidite currents with pelagic sedimentation (Glaccum and Prospero, 1980; Zaczek et al., 2015; Troll et al., 2022). Closer to Africa these sedimentary units reach thicknesses of up to 8 km, while under the Western Islands of El Hierro and La Palma they amount to only ~0.5 to 1 km in thickness (e.g., Ranero et al., 1995; Collier and Watts, 2001; Gee et al., 2001; Zaczek et al., 2015; Hunt and Jarvis, 2017). The submarine portion of Gran Canaria is not well characterized, apart from drilled hyaloclastite deposits from the sedimentary apron of the island (e.g., Schmincke and Segschneider, 1998). The interior of the island hosts a plutonic core of mafic to intermediate and even in part syenitic composition (e.g., Ye et al., 1999; Hansteen and Troll, 2003). Gran Canaria's subaerial volcanic evolution is divided into three main volcanic phases or episodes, each succeeded by an erosional hiatus (Fig. 1). The main shield building phase began during the Miocene, presumably between 16 and 14.5 Ma, and was followed by a major period of extensive felsic volcanism, which lasted from ~14 to ~8.5 Ma (McDougall and Schmincke, 1976; Cousens et al., 1990; Thirlwall et al., 1997; Schmincke and Sumita, 1998, 2010; van den Bogaard and Schmincke, 1998). Volcanism stayed dormant from ca. 8.5 Ma to 5 Ma, and was followed by the Pliocene Roque Nublo phase of small to medium-sized alkaline volcanic activity (Pérez-Torrado et al., 1995; Carracedo and Troll, 2016). The third and least voluminous phase of volcanism on Gran Canaria started in the Quaternary and continues into recent times with the last eruption occurring at ca. 1970 (±70) BP (Rodriguez-Gonzalez et al., 2009; Aulinas et al., 2010a, 2010b). The eruptive rocks that were produced by this youngest episode of volcanism on Gran Canaria are mafic alkaline nephelinites and basanites, and are predominantly found in the North and North-eastern part of the island. These recent volcanic rocks erupted in the form of cinder cones, lava flows and local hydromagmatic deposits from maars (Schmincke and Sumita, 2010; Carracedo and Troll, 2016). The frothy xenoliths (xeno-pumice) examined in this study were retrieved from a series of Quaternary to recent volcanic vent sites, namely Montañón Negro, La Isleta, Los Cernicalos, and Caldera de los Marteles (Fig. 1; cf. Hoernle, 1998; Hansteen and Troll, 2003; Rodriguez-Gonzalez et al., 2009; 2018; Schmincke and Sumita, 2010; Carracedo and Troll, 2016).

2. Methodology

2.1. Sampling

Over 50 massive to frothy xenolith samples were collected from Quaternary, recent volcanic vent sites in North and Northeast Gran Canaria. Following initial laboratory screening of the collected xenoliths, 14 representative samples from four different sites were chosen for more detailed mineralogical and oxygen isotope analysis (Table 1). The selected samples were cut for thin section preparation and a representative aliquot of each rock sample was crushed in a jaw crusher and powdered in an agate ball mill at Uppsala University, Sweden in preparation for stable isotope analysis (see below). Thin sections were investigated under a petrographic microscope and through EMPA analysis.

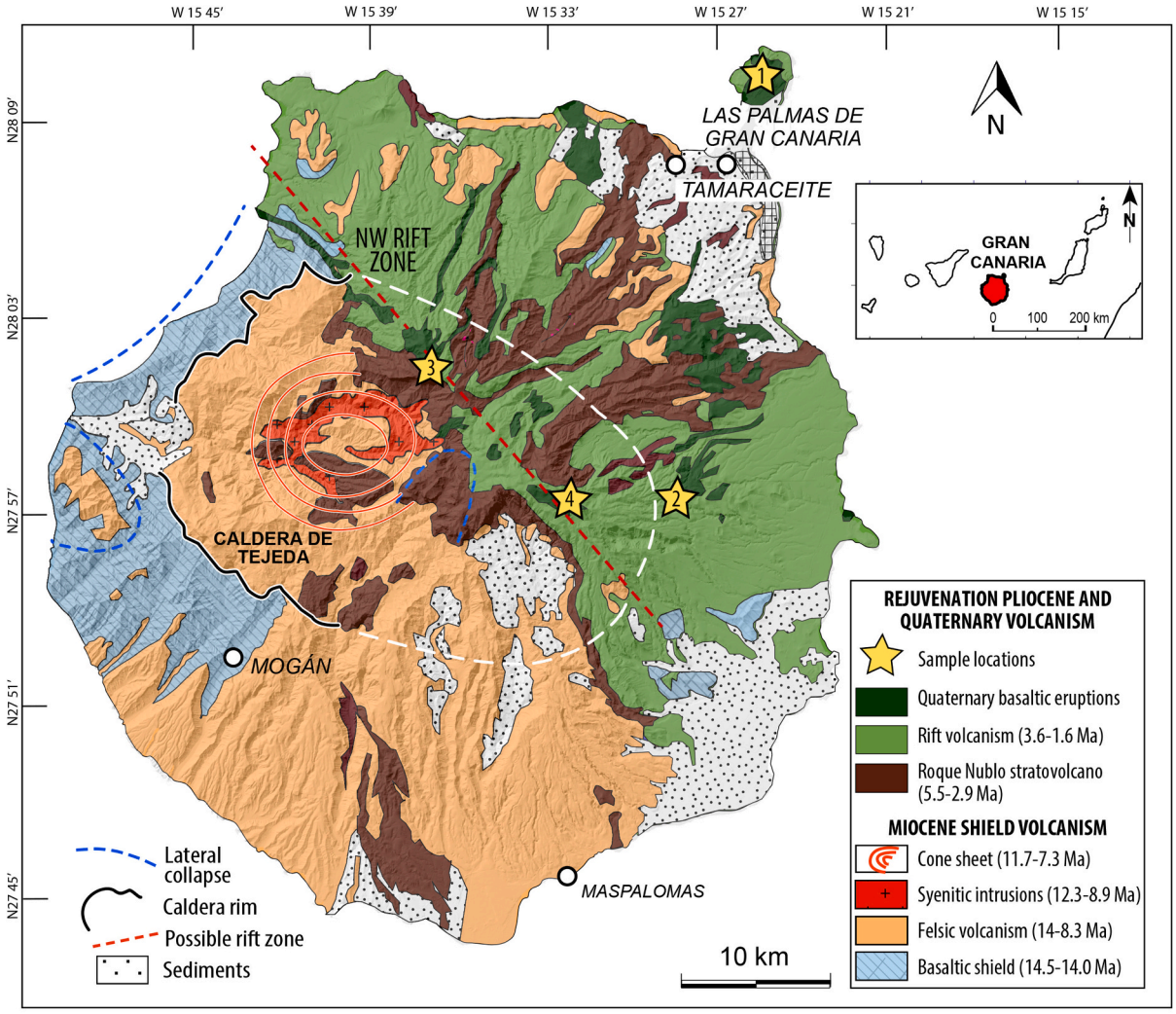

Fig. 1. Geological map of Gran Canaria, adapted from IGME (Instituto Geológico y Minero de España) and Carracedo and Troll, 2016. The majority of north-western Gran Canaria is composed by the Roque Nublo stratovolcano (brown) which lava flows extend across the Caldera de Tejeda to both east and west, and more recent volcanism including Quaternary basaltic eruptions (dark green). On the south-western portion of island one can instead find exposures of the early shield-stage volcanism, including Miocene basalts (blue) as well as felsic volcanic rock units (orange), and syenitic intrusions (red). Sample locations (marked with a yellow star) are: 1. La Isleta, 2. Los Cernicalos, 3. Montañón Negro, 4. Caldera de Los Marteles. (For interpretation of the references to colour in this figure legend, the reader is referred to the web version of this article.)

2.2. Electron microprobe analysis (EMPA)

Glass and mineral compositions were acquired from the 14 selected samples using the field emission source JEOL-JXA-8530F Hyperprobe at Uppsala University, Sweden. Analyses were conducted under standard operating conditions of 15 kV accelerating voltage and 10 nA probe current with counting times of 10 s on peak and 5 s on lower and upper background with a defocused beam of 3 to 5 μm in diameter for glass analysis, and a focused beam of 1 μm for mineral analysis. Measurements of monazite grains and age estimate calculations were performed following methods described in Montel et al. (1996) and Allaz et al. (2020). Spectrometers 1 and 2 used TAP crystals to analyze Na, Al, Si, and Mg. Spectrometer 3 collected Ti and Mn with a PETJ crystal. Spectrometer 4 analyzed K, Ca and Ba with a PETH crystal. Iron, Ni and Cr were measured on a LIFH crystal on spectrometer 5. The following standards were used for calibration; wollastonite for Ca and Si, pyrope for Si, pyrophanite ($MnTiO_3$) for Mn and Ti, magnesium oxide for Mg, orthoclase for K, albite for Na, baryte for Ba and aluminum oxide for Al, fayalite for Fe, nickel oxide for Ni and chromium oxide for Cr. Detection limits are ≤90 ppm for major elements, and ≤ 135 ppm for minor and trace elements (such as Mn, Cr and Ni). Analytical precision was verified using Smithsonian Institute mineral standards (anorthite (USNM 137041, n = 429), anorthoclase (USNM 133868, n = 550), augite (USNM 122142, n = 220), Cr-augite (USNM 164905, n = 365), Ca-plagioclase (USNM 115900, n = 240), and olivine (USNM 111312, n = 490)), which show that oxides with concentrations greater than10 wt % give uncertainties of ≤1.5 s.d, and oxides with concentrations of 5–10 wt% give uncertainties of ≤2.2% s.d.. Oxides present in lower concentrations than 5 wt% have analytical uncertainties of ≤10% s.d. Full analytical details for the EMPA are available in Barker et al. (2015) and Geiger et al. (2016).

2.3. Oxygen isotope analysis

Oxygen isotope ratios for 13 selected frothy xenoliths were acquired from whole rock powders using a Thermo DeltaXP mass spectrometer at the University of Cape Town, South Africa. Oxygen was extracted from approximately 10 mg of powdered sample that was dried at 50 °C and subsequently degassed under vacuum at 200 °C on a conventional silicate extraction line utilizing externally heated Ni vessels (Vennemann and Smith, 1990; Fagereng et al., 2008). Samples were then reacted with ClF_3, and the liberated O_2 was converted to CO_2 using a hot platinized

Table 1
Sample location, petrographic characteristics, and $\delta^{18}O$ for the analyzed xeno-pumice suite.

Sample name	Sample location	Latitude	Longitude	Colour (xenolith)	Mineralogy (xenolith)	Glass content (xenolith)	Vesicularity (xenolith)	Vesicularity (rim)	$\delta^{18}O$ (‰)	Bubble migration present?	Lithology/ Mineralogy (group)
GC-MN-XP-1	Moñtanòn Negro	28° 1′39.86"N	15°36′48.28"W	Yellowish gray to black	Qtz	20%	20%	70%	13.7	yes	Sedimentary
GC-MN-XP-2	Moñtanòn Negro	28° 1′39.86"N	15°36′48.28"W	White	Fsp, Qtz	40%	40%	no rim	4.1	yes	Igneous
GC-MN-XP-3	Moñtanòn Negro	28° 1′39.86"N	15°36′48.28"W	Light gray	Fsp	15%	10%	no rim	6.6	no	Igneous
GC-MN-XP-6	Moñtanòn Negro	28° 1′39.86"N	15°36′48.28"W	Dark gray	Fsp	25%	15%	40%	3.8	yes	Igneous
GC-MN-XP-8	Moñtanòn Negro	28° 1′39.86"N	15°36′48.28"W	Light gray to black	Fsp	45%	35%	50%	4.9	yes	Igneous
GC-MN-XL-1	Moñtanòn Negro	28° 1′39.86"N	15°36′48.28"W	Light gray to whiteish	Fsp	5%	2%	no rim	3.6	no	Igneous
GC-MN-XL-9	Moñtanòn Negro	28° 1′39.86"N	15°36′48.28"W	Brownish to gray	Fsp	5%	5%	no rim	4.9	yes	Igneous
GC-ElH-XP-2	Los Cernicalos	27°57′52.59"N	15°29′18.65"W	Dark ochre	Qtz	10%	20%	50–60%	16.0	yes	Sedimentary
GC-ElH-XP-4	Los Cernicalos	27°57′52.59"N	15°29′18.65"W	Light gray to black, ochre	Qtz	20%	30%	50%	16.3	yes	Sedimentary
GC-Li-XP-1	La Isleta	28° 9′49.86"N	15°24′55.88"W	Ochre	Qtz	30%	40%	50%	14.5	yes	Sedimentary
GC-SS1-XP-1	C. d. Los Marteles	27°57′7.68"N	15°31′43.45"W	Whiteish to light gray	Qtz	40%	40%	75%	15.1	yes	Sedimentary
GC-SS1-XP-4	C. d. Los Marteles	27°57′7.68"N	15°31′43.45"W	Light gray, ochre	Qtz	30%	35%	75%	8.1	yes	Sedimentary
GC-SS2-XP-1	C. d. Los Marteles	27°57′7.68"N	15°31′43.45"W	Ochre	Qtz	15%	10%	no rim	16.8	yes (?)	Sedimentary
GC-SS2-XP-1.2	C. d. Los Marteles	27°57′7.68"N	15°31′43.45"W	Gray	Qtz	40%	25%	50%	N/A	yes	Sedimentary

carbon rod. Unknowns were run with duplicates of the internal quartz standard (MQ) which was used to calibrate the raw data to the SMOW (Standard Mean Ocean Water) scale, using a $\delta^{18}O$ value of 10.1 for MQ (calibrated against NBS-28). All $\delta^{18}O$ results are reported in standard δ-notation, where $\delta = (R_{sample}/R_{standard} - 1)$ x 1000 and $R = {}^{18}O/{}^{16}O$. The analytical error is estimated as ±0.2‰ (2σ) based on long-term repeated analysis of MQ.

3. Results

3.1. Textural analysis

The studied xenolith samples have been inspected for their petrographic features and the key observations are summarized in Table 1. Variations in colour of the collected xenoliths range from white over different shades of yellow to orange and various shades of gray (Fig. 2C-N). Vesicle content also differs between samples. Some of the inspected xenoliths are relatively massive, while the majority is frothy, highly friable and crumble under light pressure. Vesicularity of the xenoliths ranges from <5% to >50%, and higher vesicularity is generally observed to correlate with higher glass content (Table 1). Coalesced bubbles forming bubble migration paths (elongated vesicle trails) (cf. Berg et al., 2016) can be observed in most (12 of 14) of the studied xenoliths (Fig. 3C-D; 4C). We refer to the frothy xenoliths of this study as "xeno-pumice" (XP) following the definition of Troll et al. (2012) and Gardner et al. (2013), but also include some massive examples with less vesicular textures (<5% vesicle content; Table 1) in this suite to represent the earliest stages of vesiculation.

The basaltic material (hereafter referred to as "crust" or "rim") attached to some of the xenoliths is usually vesicular (vesicle content ~40 to 75 vol%; Table 1). At contacts with the xenolith samples, the vesicles in the basaltic crust tend to be considerably larger (Fig. 3A-C), whereas within the xenolith specimens vesicles range in diameter from <1 mm to almost 1 cm in exceptional cases and may be concentrated in bands or distributed evenly throughout the samples (various vesicle morphologies are represented in Figs. 2, 3, and 4).

In BSE images the frothy samples display relict crystals and abundant bubbles associated with glassy domains (Figs. 4, 5). Frequently, thin films of glass are present throughout the xenoliths, but larger glass domains have locally segregated, which usually host comparatively large bubbles (Figs. 3, 4, 5). These textures are similar to those observed in samples from e.g., Anak Krakatau, Lanzarote, La Palma, and at El Hierro (e.g., Aparicio et al., 2006; Troll et al., 2012; Gardner et al., 2013; Carracedo et al., 2015; Carracedo and Troll, 2016; Graettinger et al., 2020).

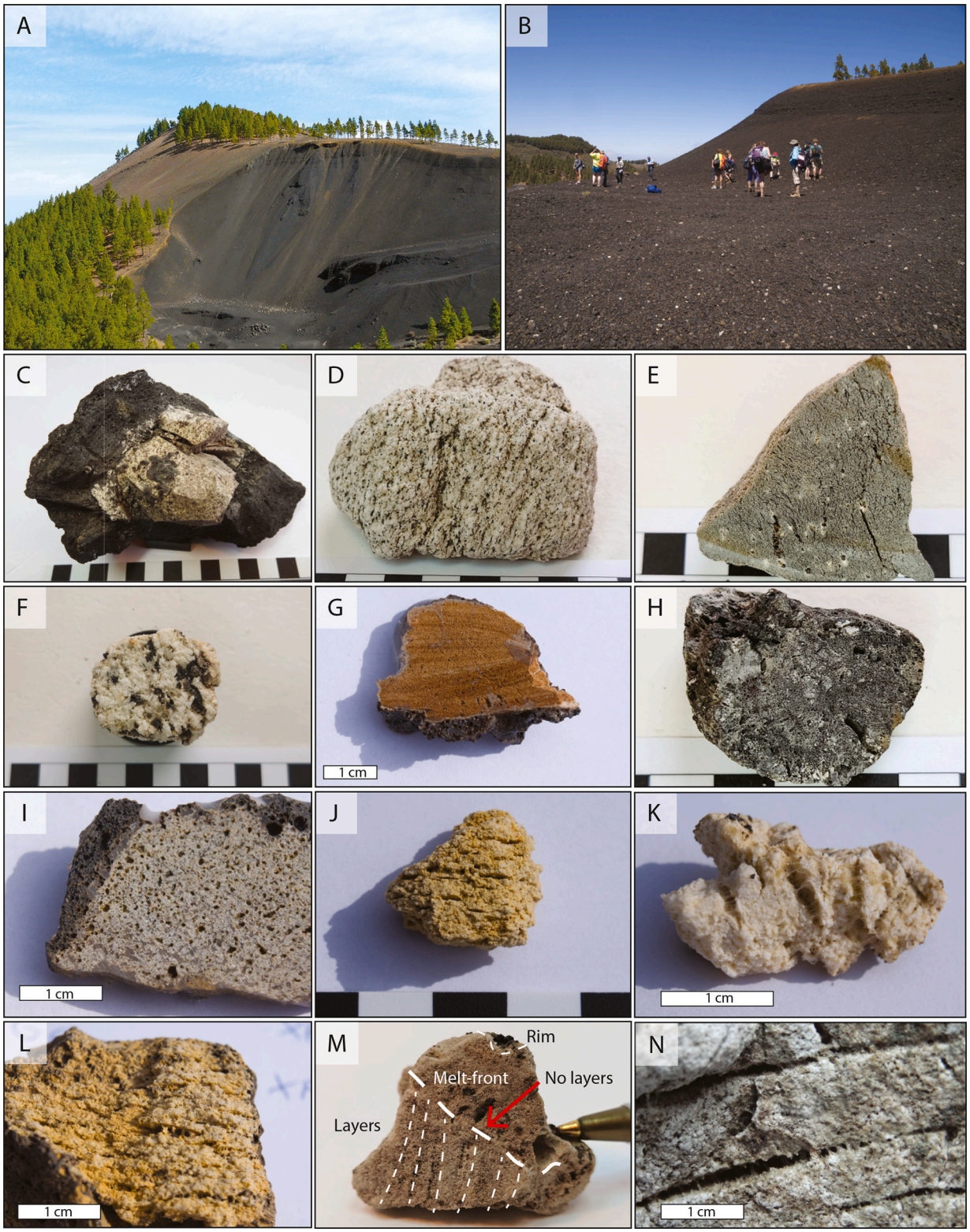

Fig. 2. A-B. Lapilli quarry at Montañón Negro. The quarry is located within a quaternary eruption site, and is one of the sample sites for xeno-pumice on Gran Canaria (eruption age ~ 3 kyrs BP; Rodriguez-Gonzalez et al., 2009). The xeno-pumice can be seen as small, light dots on the darker ground. C—K. Collected xeno-pumice samples of various mineralogy (quartz-rich and feldspar-rich) sorted in increasing vesicularity, showing the broad variation of colour (white, yellow, orange to dark gray), basaltic rims (dark gray to black), and varying vesicle morphology (heterogeneous to homogeneous vesicle distribution and sizes vesicle trails). L-N. Vesiculation along layer boundaries. M. Quartz-rich xeno-pumice composed of two sections; 1. Primary layering (marked with thin dashed line), and 2. No layers and homogenous vesiculation at the contact with the basaltic melt (rim). Textural separation is a result of higher melt-degree at rim-contact, and a relatively unaffected core. The two sections are separated by a highly vesiculated melt/degassing-front. (For interpretation of the references to colour in this figure legend, the reader is referred to the web version of this article.)

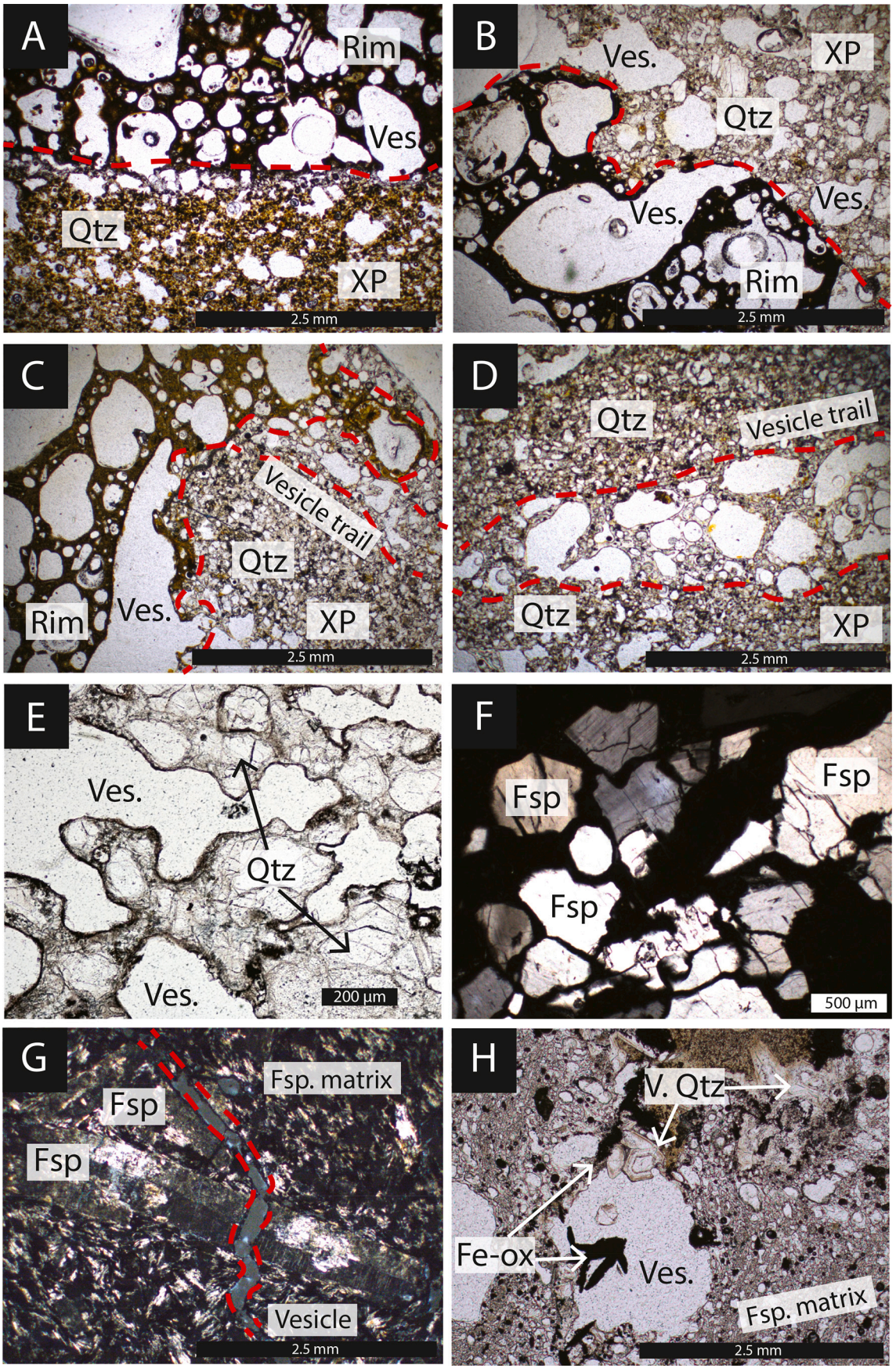

(caption on next page)

Fig. 3. Microphotographs of xeno-pumice and associated mafic rims. A-C. Basaltic melt (now mafic glass) constituting the rim (dark brown, porphyritic), interacting with quartz-rich xeno-pumice (fine-grained, lighter colored). The contact between the xeno-pumice and mafic glass is at times vesicular and may show a variety of textures, ranging from occurrence of small bubbles (A) to larger, and at times coalesced vesicles and vesicle trails (B and C). Plane-polarized light. D. Bubble migration and consequent vesicle trail in a frothy, fine-grained matrix of a quartz-rich xeno-pumice. Plane-polarized light. E. A glassy, frothy xeno-pumice constituting mainly anhedral quartz crystals. Plane-polarized light. F. Feldspar-rich (phaneritic) portion of a relict domain in xeno-pumice. Crossed-polarized light. G. Xeno-pumice with cloudy, i.e. mildly altered, K-feldspar phenocrysts in feldspar-rich matrix with trachytic texture. Vesiculation mainly occurs in between fracture planes (here seen in the fractured phenocryst) or along grain boundaries. Crossed-polarized light. H. Xeno-pumice with feldspar-rich, trachytic matrix, and secondary quartz crystals as vesicle infills. The quartz crystals are euhedral to subhedral and normally zoned, indicating that they are a product of late stage vapor phase crystallization (V. Qtz in figure). Euhedral iron oxides are also precipitated within the vesicle cavities. Plane-polarized light. (For interpretation of the references to colour in this figure legend, the reader is referred to the web version of this article.)

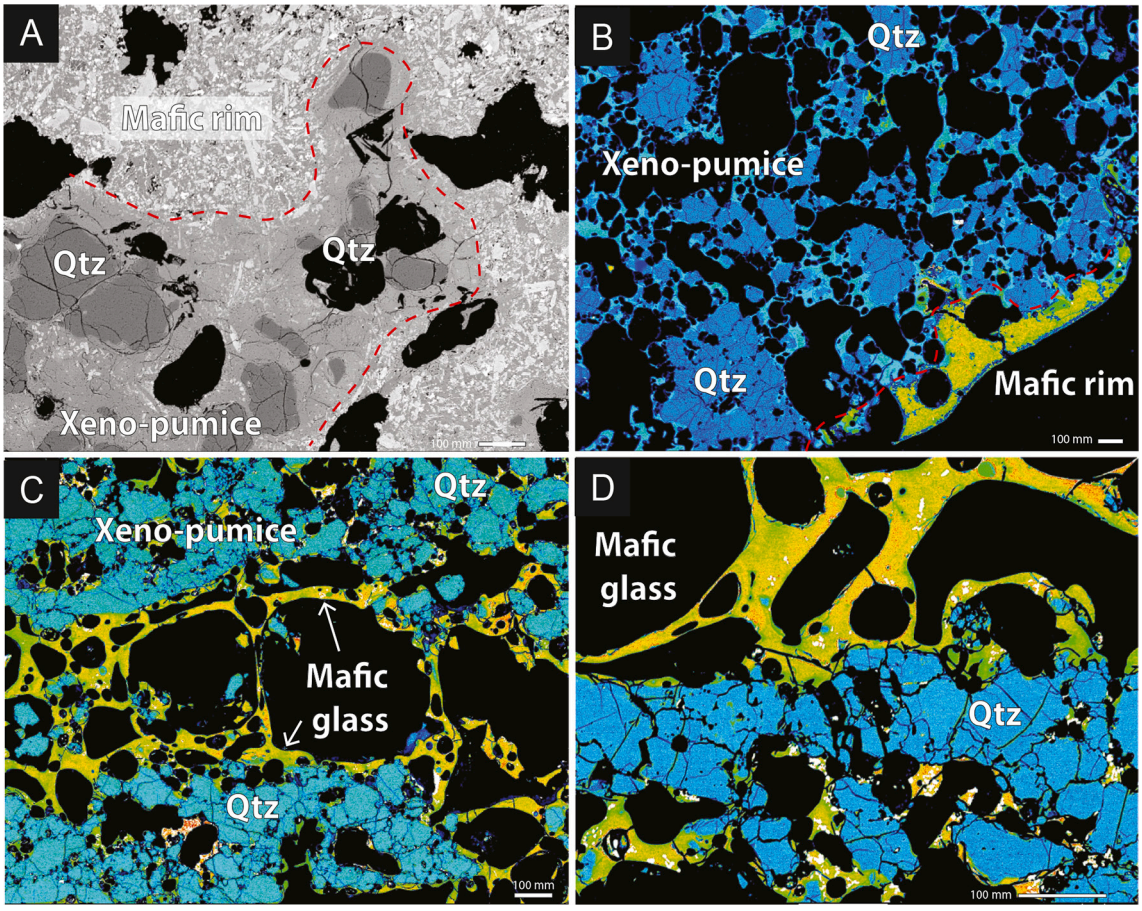

Fig. 4. Back scattered electron (BSE) images of glassy textures and interaction of intruding basaltic melt and quartz-rich xeno-pumice. Retrieved with microprobe, in BSE true colour (gray scale), and false colour mode (blue for fsp and qtz; green, yellow, orange, and white for denser minerals). Vesicles can be seen in black. A. Partial melting and assimilation of quartz-rich xenolith into mafic domain (mafic rim). B. Quartz-rich xenolith with vesicles and intact mafic rim. C. Vesicle trail and quartz grains aligned with migrated mafic glass (light green). D. Close up of vesiculated mafic glass and quartz grains. (For interpretation of the references to colour in this figure legend, the reader is referred to the web version of this article.)

3.2. Mineralogical analysis

The dark brown to black basaltic crust encapsulating the xenoliths contains olivine, clinopyroxene and some orthopyroxene phenocrysts set in a finely crystalline to glassy matrix (Fig. 3A-C; 4A-B). Basaltic glass, containing olivine, pyroxene and plagioclase microcrystals, can also be found to have intruded several of the frothy xeno-pumice specimens (Fig. 4C-D). The investigated xeno-pumice, in turn, show a wide range of mineral assemblages that comprise feldspar, pyroxene, clay minerals, euhedral and anhedral Fe—Ti oxides, sphene, jasper, and quartz that are set in a finely crystalline to glassy groundmass with glass contents between 5 vol% and up to almost 50 vol% (Figs. 3, 4, 5; Table 1).

The examined xeno-pumice can be further divided into two separate groups according to petrographic features, and especially on the basis of their mineral contents.

The first group consists of six xenoliths from Montañón Negro that contain predominantly feldspar crystals, commonly found as euhedral phenocrysts and megacrysts (>5 mm) showing Carlsbad twinning, situated in a solid grayish to beige fine grained to glassy groundmass (Table 1; Fig. 3G; 5D). The megacrysts often display cloudiness and are commonly fractured. Minor amounts of small nepheline or apatite phenocrysts are also observed. The glassy matrix mainly contains quenched, dendritic feldspar microlites, resembling trachytic textures (cf. Lofgren, 1974), and opaque oxides that are seemingly aligned along flow directions. This group is less vesicular and less glassy and was exclusively sampled at Montanon Negro (Table 1).

Textural variations in this group are particularly evident in two of the samples (GC-MN-XP-2 and GC-MN-XP-3). Sample GC-MN-XP-2 has, in addition to the microcrystalline feldspar, isolated groups of quartz

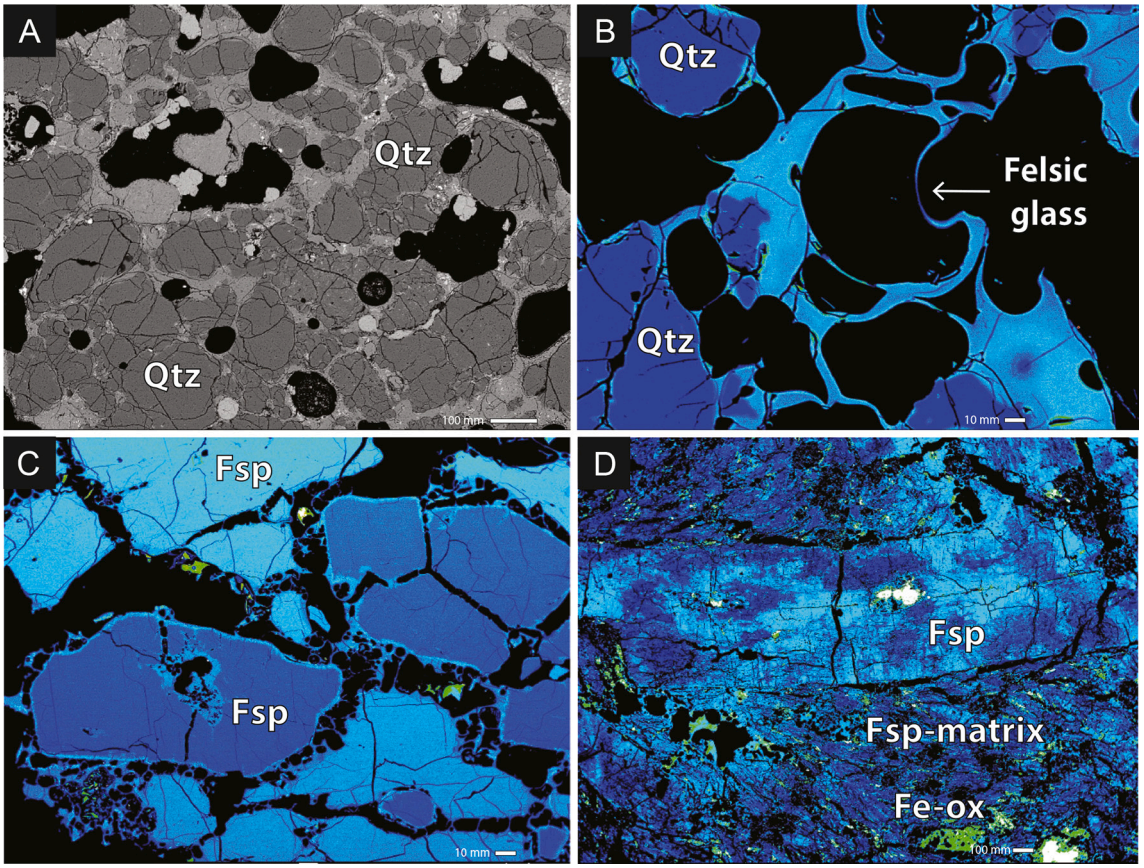

Fig. 5. BSE images of the xeno-pumice main mineralogy. Retrieved with microprobe, in BSE true colour (gray scale), and false colour mode (blue for Fsp and Qtz; green, yellow, orange, and white for denser minerals). Vesicles can be seen in black. A. Intact quartz grains with relatively little vesiculation and small/no space between grains. B. Quartz grains almost completely separated due to degassing and vesiculation, and partly disorganized grain boundaries. C. Phaneritic feldspar-rich sample showing crystals with minor reaction rims (lighter in colour) separated by vesiculation and thin glass film along grain boundaries. D. Patchy alteration and fracturing in feldspar megacrysts that reside in a microcrystalline matrix. Localized vesiculation along grain boundaries is already present. (For interpretation of the references to colour in this figure legend, the reader is referred to the web version of this article.)

crystal agglomerates (Fig. 3H). These quartz grains are euhedral and zoned, and occupy (partly or fully) vesicles of the sample (Fig. 3H). However, this observation is reminiscent of vapor phase crystallization, a process taking place when acid volcanic gasses react with already present minerals and deposit silica within pores or fractures in the form of impure cristobalite (eg. Schipper et al., 2020), i.e., a secondary mineral phase. Sample GC-MN-XP-3 is, in turn, phaneritic and consists mainly of unaltered feldspar grains, which show only minor reaction rims at the glass boundary (Fig. 3F, 5C).

In contrast, a second group of eight xenoliths contains dominantly small (<0.5 mm) mineral grains, with local secondary overprint textures (Table 1; Fig. 3A-E; 4A-D; 5A-B). Quartz is the most common mineral in this group, with accessory minerals being feldspar, clay minerals, jasper, various Fe—Ti oxides, monazite and zircon. The quartz grains are generally anhedral, non-zoned, and homogeneous in size within individual samples. Another notable feature are the layered textures where vesicle trails traverse distinct layers, indicating later fluid and volatile migration that transgressed the primary layering (Fig. 2G, and M-N). This group of xenoliths thus differs from the first one as the samples are rich in quartz, and lack the fractured feldspar phenocrysts as well as the trachytic texture of microcrystalline feldspar in the glassy matrices (Table 1).

On the bases of the mineralogy and textures described above we observe two broad groups; one displaying characteristics of magmatic rocks, thus termed the '*Magmatic Group' (Group I: trachytic texture and abundant feldspar phenocrysts*), and another group that dominantly shows sedimentary features, thus termed the '*Sedimentary Group'* (*Group II: rounded quartz grains, clay minerals, jasper*) .

3.3. Glass composition

The analyzed xenolith glass domains exhibit high variability in silica content, ranging from 44.8 wt% to 100.0 wt% SiO_2 with an average of 70.6 wt% SiO_2 for the full range of investigated xeno-pumice samples (Supplementary Table 1). It should be noted that the highest measured silica contents of 100 wt% SiO_2 ($n = 30$) are found in the glass of sample GC-SS2-XP-1. The measured xenolith glass further shows a wide distribution of all major element oxides, which often partially overlap with the basaltic glass compositions (Figs. 6, 7). Xeno-pumice group I samples (i.e., feldspar-rich) show overall lower SiO_2 contents (44 to 69 wt%), contrasting the glass in the group II sedimentary xeno-pumice which have silica contents of 58 to 100 wt%.

In addition, the glass of the eight group II sedimentary xenoliths also shows elevated contents of FeO (average of 2.85 wt% for group II, while magmatic group I from Montañón Negro shows an average of 0.3 wt%) (Fig. 7). Moreover, the xeno-pumice in group I ($n = 6$, from Montañón Negro) have higher alkali content (averages of 9.4 wt% K_2O and 4.23 wt % Na_2O), and aluminum content (19.4 wt% Al_2O_3 average) than the quartz-rich group II xeno-pumice samples ($n = 8$) with averages of 11.4 wt% Al_2O_3, 1.8 wt% K_2O, and 3.57 wt% Na_2O) (Fig. 7).

The glass of the mafic rims ($n = 9$) around all investigated xenoliths record an average silica content of 49.6 wt% SiO_2 and plot mainly in the basanite field on the total alkali vs. silica diagram, similar to recent Gran Canaria volcanics (e.g., Aulinas et al., 2010a, 2010b; Fig. 6), but some of

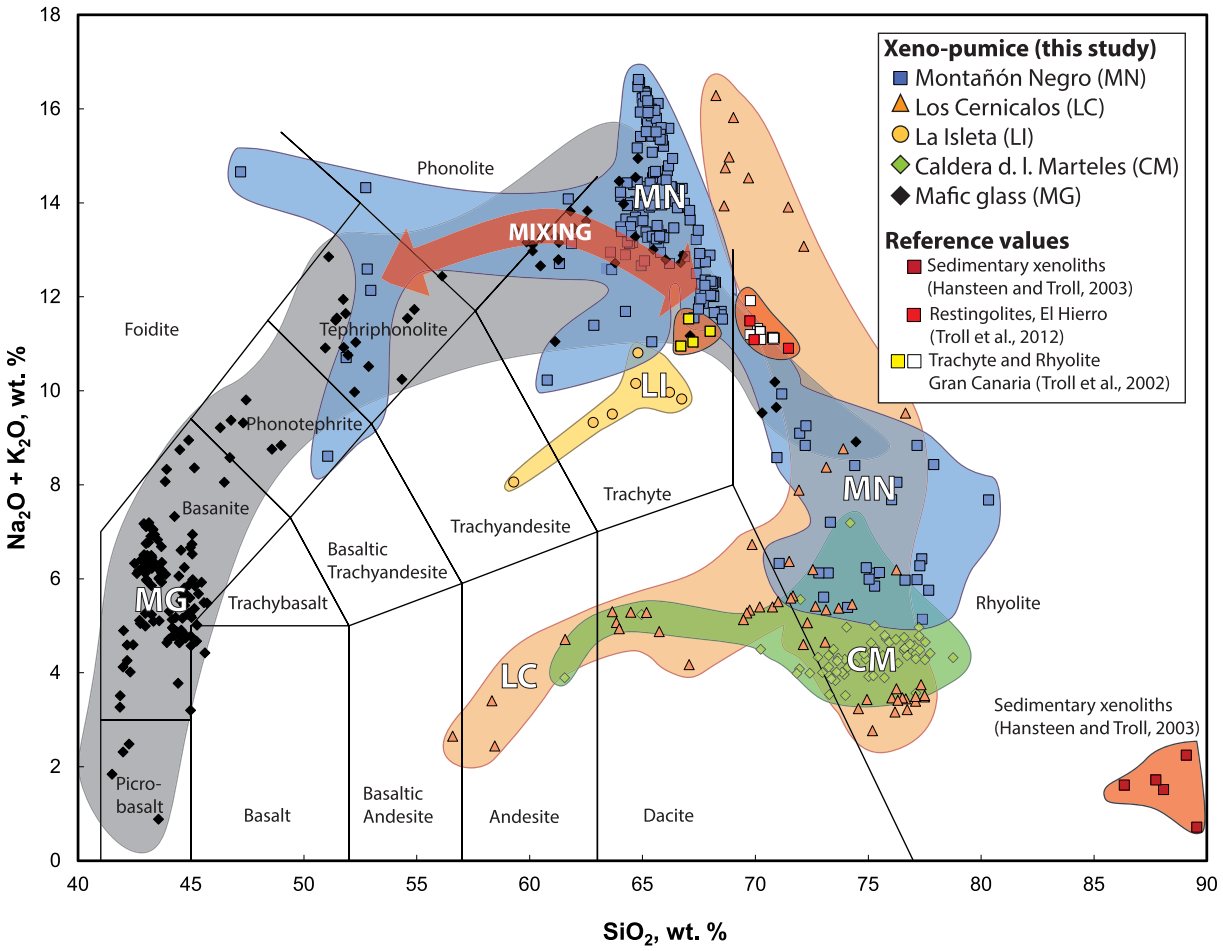

Fig. 6. Total alkali vs. SiO_2 wt% diagram, with fields after Le Bas et al. (1986). The various xeno-pumice glasses (blue, yellow, orange and green clouds) plot mainly in the trachyte and rhyolite fields, showing a larger compositional diversity than literature whole rock data of rhyolite, trachyte (Gran Canaria), and restingolites (El Hierro) (red clouds). Mixing between the glass of the mafic rim (black) and xeno-pumice follows a mixing trend from mafic to felsic, where the chemical diversity is traceable in both mafic and xeno-pumice glass regimes. Group affinity of individual samples is provided in Table 1. (For interpretation of the references to colour in this figure legend, the reader is referred to the web version of this article.)

the rim glasses exhibit a considerable compositional variability in SiO_2 contents ranging from 39.6 to 74.5 wt%. Similar variability is also seen in the other major element oxides (Fig. 7).

3.4. Oxygen isotopes

The $\delta^{18}O$ values of the xenolith samples range from 3.6 to 16.8‰ and strongly exceed the common range of ~5.5 to 7‰ in fresh igneous rocks (Taylor, 1968; Bindeman, 2008; Bindeman et al., 2022). The new data are shown with reference values for altered and unaltered basalt, syenites, hydrothermally altered trachyte, and sedimentary xenoliths from Gran Canaria, 'restingolites' from El Hierro, and the mean mantle value (Fig. 8 and Table 1) (Savin and Epstein, 1970a, 1970b; Taylor et al., 1967; Thirlwall et al., 1997; Bindeman, 2008; Troll et al., 2012). The $\delta^{18}O$ values are consistent with the mineralogical and textural groups; the lower range (3.6 to 6.6‰) is observed in feldspar-rich samples of Group I, and the higher range (8.1 to 16.8‰) is recorded for the quartz-rich samples of Group II (Table 1). Given the glass data and mineralogical assemblages outlined above, we recognize that near-surface alteration after deposition does not play a significant role, and thus consider the oxygen isotope values to be broadly reflective of their original lithologies prior to melting and vesiculation in the magmatic conduit.

3.5. Monazite ages

The presence of monazite allows for preliminary dating of the material making up the xeno-pumice samples (cf. Montel et al., 1996). Several monazites were analyzed but only measurements of one monazite in sample GC-SS2-XP-1.2 (quartz-rich xeno-pumice of Group II) could provide a reliable calculated age. The calculated age of the monazite in GC-SS2-XP-1.2 yields 600 ± 75 Ma which is contemporaneous with continental, Precambrian rock and not with the initiation of subaerial volcanism at Gran Canaria at ca. 14 Ma (e.g., McDougall and Schmincke, 1976).

4. Discussion

4.1. Classification of the massive to frothy xenoliths from Gran Canaria

The collated sample suite of xeno-pumice presents a heterogenous group, although the samples share some common petrological and geochemical characteristics such as high silica contents (>55 wt% average silica), variable vesicularity, and the often elongated vesicle trails that indicate advanced partial melting and associated degassing of the melt on volatile saturation to form vesicles in xenolith glass during ascent (cf. Troll et al., 2012; Berg et al., 2016). They also share a highly variable glass composition between xenolith glass and host rock. Measurements of the basalt rim glass, for example, follow the silica

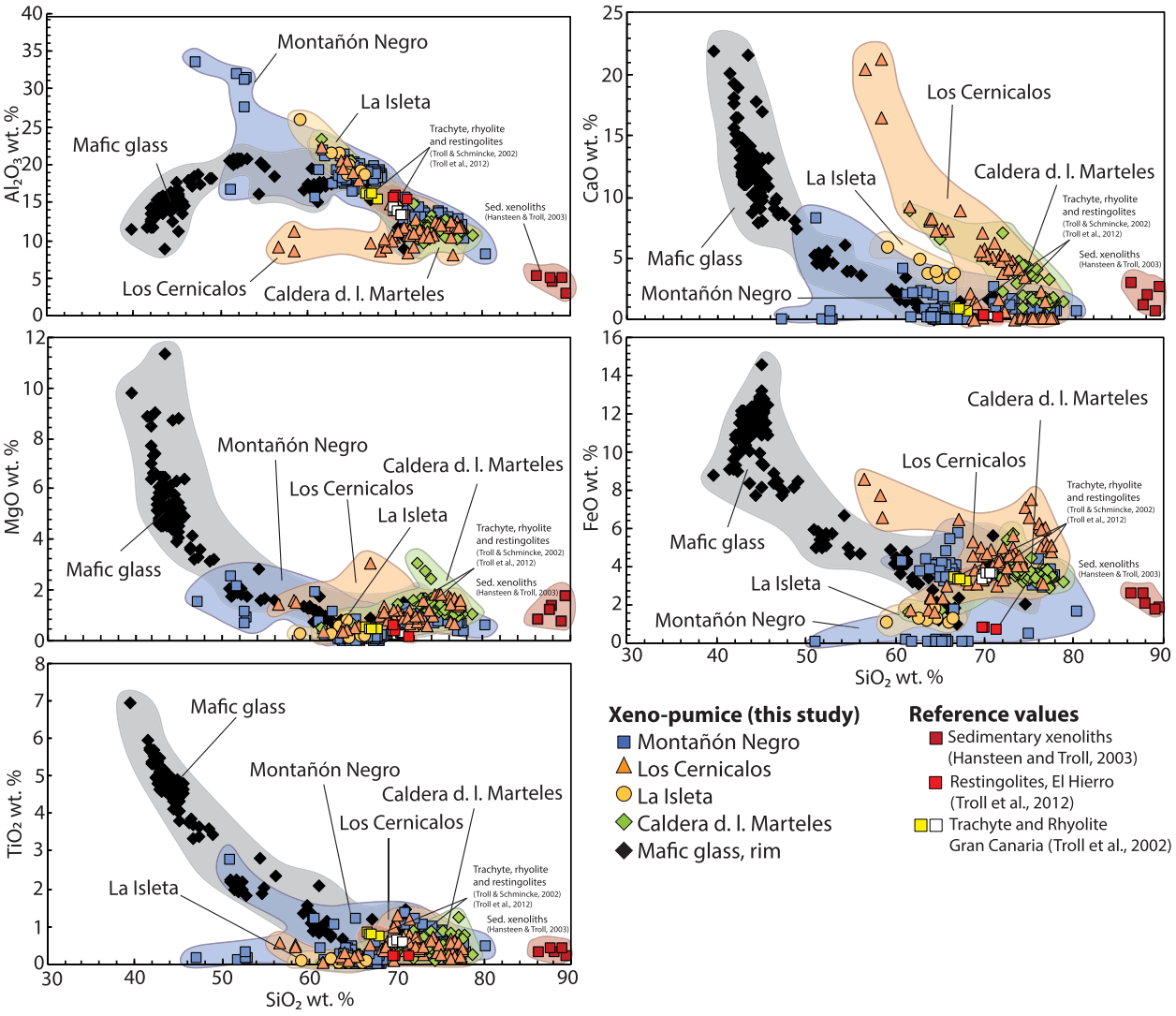

Fig. 7. Harker plots showing variations of selected major element oxides in xeno-pumice and basaltic glass, plotted against SiO_2 and compared with reference rocks from Gran Canaria and El Hierro. *Data sources: sedimentary xenoliths (whole rock), Gran Canaria (Hansteen and Troll, 2003), trachyte and rhyolite, Gran Canaria (Troll and Schmincke, 2002), and 'Restingolites' (El Hierro xeno-pumice; Troll et al., 2012).*

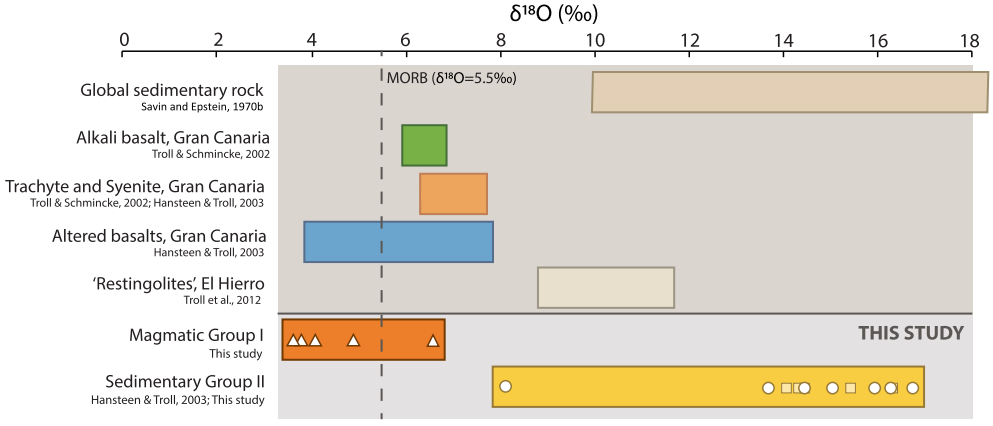

Fig. 8. Isotope oxygen values ($\delta^{18}O$, ‰) for Gran Canaria Group I and II (magmatic and sedimentary) xenoliths and xeno-pumice, and reference rocks. *Data sources: Altered basalts, sedimentary xenoliths (yellow squares), and trachyte, Gran Canaria (Hansteen and Troll, 2003), Syenite and alkali basalts, Gran Canaria (Troll and Schmincke, 2002), and xeno-pumice (restingolites) from El Hierro (Troll et al., 2012).* (For interpretation of the references to colour in this figure legend, the reader is referred to the web version of this article.)

undersaturated – alkalic trendline from picrobasalt to phonolite, up to about 68 wt% SiO_2 where the data points fall into the rhyolitic field (Fig. 6). This variation could record a snapshot of localized mixing between the silica rich xeno-pumice and mafic melt during ascent (cf. Aparicio et al., 2006, 2010). Upon entrainment and heating, physical mixing of the two melts (now glasses) is further visible at direct contacts between xenolith and mafic glass, and the latter is frequently seen to have penetrated the xeno-pumice specimens (Figs. 3, 4). Although the samples described above share similarities, they display distinct characteristics in respect to magmatic vs. sedimentary mineral assemblages. Moreover, they also show distinct glass composition ranges, and oxygen isotope ranges. Thus, we will focus our subsequent discussion on the origin of two main groups which we name magmatic (Group I, feldspar rich) versus sedimentary (Group II, quartz rich).

4.2. Group I - magmatic xenoliths

Group I xenoliths of this study are only found at the Montañón Negro sample site, and consist dominantly of feldspar. The six samples of Group I show a typical igneous mineralogy, which includes euhedral but cloudy feldspar phenocrysts, and smaller feldspar crystals aligned in a trachytic flow texture (Fig. 3G; 4D). Although quartz is not absent in this group (Table 1), it is only observed in one sample (GC-MN-XP-2) and these quartz crystals are distinctly different from those in Group II. Instead, the quartz of GC-MN-XP-2 is most likely the result of a secondary vapor phase crystallization, as the grains are strongly zoned, euhedral to subhedral, and occur as infill inside vesicles (Fig. 3H; cf. Schipper et al., 2020). The presence of secondary quartz in this specific sample must thus not be confused with primary detrital quartz of sedimentary origin. All xenoliths of Group I furthermore present a lower range of average glass silica content (ca. 65 wt% SiO_2), falling mostly into the trachyte field in the TAS diagram (Fig. 6). The magmatic xenolith group also does not overlap with the whole rock compositions known for sedimentary xenoliths from Gran Canaria (cf. Hoernle, 1998; Hansteen and Troll, 2003), hence further arguing for a non-sedimentary origin.

The $\delta^{18}O$ values (3.6 to 6.6‰) of the magmatic Group I xenoliths are similar to values obtained for whole-rock igneous samples from the Canary Islands (cf. Troll and Schmincke, 2002; Hansteen and Troll, 2003; Deegan et al., 2012), and are, therefore, unlikely to be sedimentary in origin. Moreover, the $\delta^{18}O$ values of the magmatic group are mostly below the mean mantle value of 5.5‰ (Cooper et al., 2009), with the lowest value being 3.6‰ (Fig. 8). All xenoliths with oxygen isotope ratios lower than 5‰ have trachytic textures, often cloudy feldspar phenocrysts and average SiO_2 glass contents below 70 wt% (Fig. 9). The low $\delta^{18}O$ values may have been caused by high-temperature hydrothermal alteration (see Hansteen and Troll, 2003; Donoghue et al., 2008, 2010), and the low $\delta^{18}O$ xenoliths could reflect earlier high-temperature hydrothermal alteration within the volcanic edifice (cf. Taylor et al., 1967; Hansteen and Troll, 2003; Donoghue et al., 2010) (Fig. 7). Such interaction is also recorded in rocks found within the Tejeda caldera in central Gran Canaria, that display a range of high to low $\delta^{18}O$ values, caused by interaction of hydrothermal fluids and alteration (Donoghue et al., 2010). The xenolith group with lower $\delta^{18}O$ values (3.6 to 6.6‰) overlaps with unaltered and high-T altered igneous material from Gran Canaria (4.1 to 7.7‰), the lowest values being present in the altered material (eg. Cousens et al., 1990; Troll and Schmincke, 2002; Hansteen and Troll, 2003; Donoghue et al., 2010). We conclude that xenoliths with $\delta^{18}O$ values lower than the mantle (5.5‰) measured in this study (3.6 to 4.9‰) thus represent high temperature altered igneous rocks (e.g., Donoghue et al., 2010; Berg et al., 2018).

On the other hand, sample GC-MN-XP-3 has a $\delta^{18}O$ value of 6.6‰, a plutonic texture, and shows little to no alteration of the feldspars (Fig. 3F;5C). This sample is likely a syenitic xenolith (i.e a plutonic lithology) that has experienced only limited high-temperature alteration prior to magmatic entrainment, in comparison to the other, low-$\delta^{18}O$ xenoliths of the group that are significantly altered. Group I magmatic xenoliths probably represent a range of intermediate to felsic rocks from previous magmatic episodes from the island's volcanic edifice that have experienced various degrees of alteration, partial melting and degassing prior to eruption.

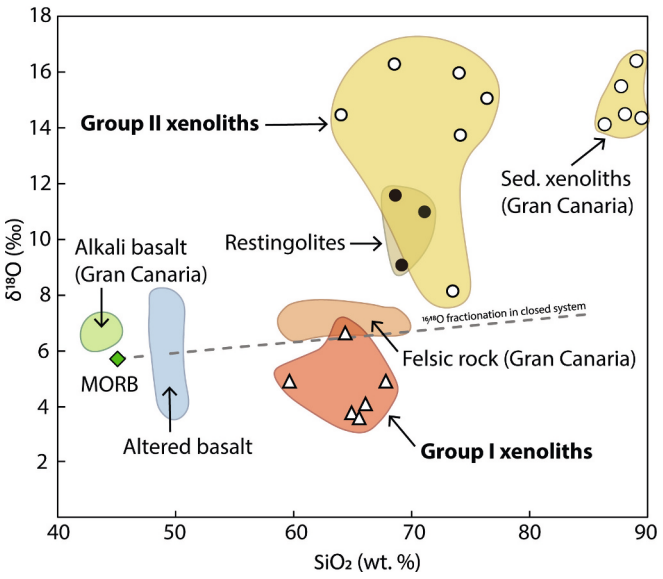

Fig. 9. Plot of $\delta^{18}O$ versus SiO_2 average for xeno-pumice glass. The magmatic Group I (triangles) plot below the expected trajectory for Rayleigh fractionation within a closed system (dashed line; Bindeman, 2008) from a MORB value of 5.7‰ (green diamond) in respect to increased silica content. The sedimentary Group II (circles), in contrast, plot above the same trajectory. *Altered basalts* (Thirlwall et al., 1997; Hansteen and Troll, 2003), *Sedimentary xenoliths* (Troll and Schmincke, 2002; Hansteen and Troll, 2003), *Alkali basalt* (Troll and Schmincke, 2002), *and El Hierro xeno-pumice ('Restingolites')* (Troll et al., 2012). (For interpretation of the references to colour in this figure legend, the reader is referred to the web version of this article.)

4.3. Group II - sedimentary xenoliths

Eight of the 14 selected xeno-pumice samples show sedimentary features (Table 1). This observation is based on mineralogy (quartz, clay minerals, and a considerable heavy mineral fraction of zircon and monazite), and layered textural characteristics (see Results). In addition, the non-magmatic mineral assemblage and textures in this group coincide with high concentrations of SiO_2 in the xenolith glass (>75 wt% average) and high $\delta^{18}O$ values (8.1 to 16.8 ‰) (Figs. 8 and 9) that overlap with the accepted range (9 to 30‰) for sediments in general (cf. Savin and Epstein, 1970a, 1970b; Hansteen and Troll, 2003; Troll et al., 2012; Carracedo et al., 2015). Moreover, the high $\delta^{18}O$ value group shows a similar range to previously identified sedimentary xenoliths from the region (e.g., Troll and Schmincke, 2002; Hansteen and Troll, 2003; Troll et al., 2012; Rodriguez-Losada et al., 2015), and we thus consider this group to represent materials of the sedimentary portion of the pre-island oceanic crust. This conclusion is underlined by the presence of quartz, since magmas on Gran Canaria are normally silica undersaturated, and quartz is therefore not a primary magmatic phase on the island (Carracedo and Troll, 2016).

A pilot date of monazite in group II xenoliths yields an age of ~600 Ma ± 75 Ma. This Precambrian age indicates that the material composing the group II xeno-pumice was derived from pre-volcanic sediments that are formed by sediment grains originally derived from the Precambrian continental crust of mainland Africa (e.g. Glaccum and Prospero, 1980; Troll et al., 2022), rather than from much younger ocean island volcanism forming the Canary archipelago. Therefore, considering mineralogy, glass chemistry and oxygen isotopes and the

attained monazite age, we suggest that group II xenoliths are derived from continentally derived pre-volcanic sedimentary strata beneath the island edifice of Gran Canaria. This ~2 km thick strata was previously detected via geophysical studies (e.g., Ye et al., 1999; Krastel and Schmincke, 2002), and could also be the origin for similar sedimentary xenoliths that were previously described from Gran Canaria, Lanzarote, and El Hierro (Rothe and Schmincke, 1968; Aparicio et al., 2006; Aparicio et al., 2010; Troll et al., 2012; Carracedo et al., 2015). The El Hierro xeno-pumice samples in the 2011 eruption also contained remnant quartz crystals in addition to jasper fragments, wollastonite and nannofossils (Coccolithophores), and their relatively high oxygen isotope values imply that they are also of sedimentary origin (Troll et al., 2012; Rodriguez-Losada et al., 2015; Zaczek et al., 2015; Berg et al., 2016). During the 2011 El Hierro eruption, lateral magma transport over several kilometers took place within the sedimentary portion of the ocean crust allowing for extensive magma-crust interaction in the days before the eruption commenced (González et al., 2013). Notably, El Hierro xeno-pumice samples were erupted for one week only, implying that once the magmatic pathway was established, no more crustal xenoliths were entrained in the ascending magma during this specific event. This implies that crustal material under the island represents a finite reservoir. The El Hierro xeno-pumice suite together with the Gran Canarian xenoliths suite may thus help to explain and provide additional insight into the island's structure and pre-eruptive substrate, as well as changes that take place during magmatic activity.

5. A model for xeno-pumice formation on Gran Canaria

As the source region for oceanic crust sediment lies at ca. 10 km depth beneath the island (Ye et al., 1999) and is not directly accessible to

Fig. 10. Photographs of pillow lavas interacting with sediments at Tamaraceite, NE Gran Canaria. This outcrop (described in detail by Perez-Torrado et al., 2014, and Carracedo and Troll, 2016) offers an analogue to xeno-pumice formation at greater depths, as it shows frothed up marly sedimentary rock next to intruding pillow basalts (A, B). Close-up, the difference between the partly intact, layered sediments and the now frothy portion clearly depicts the effect of degassing and partial melting of the sediment as primary textures, such as layering, are replaced with a glassy network of vesicles, glass, and surviving mineral grains closely resembling sedimentary xeno-pumice (C). Partial melting and vesicle formation and migration in the partially intact sediment is also observed along less refractory layers (red arrows to the right), whereas more resistant layers are not affected. Note that the direction of the vesicle migration along the layer boundaries is nearly perpendicular to the vesicle migration in the xeno-pumice-like portion, indicating non-homogeneous degassing of the sediments. The lava-sediment interaction observed here reveals xeno-pumice formation processes (melting and vesiculation) which are also applicable to sub-surface levels. (For interpretation of the references to colour in this figure legend, the reader is referred to the web version of this article.)

us, we must rely on theoretical concepts, deductive observations, and possible analogues exposed on-shore. The process of disintegration and partial melting of xenoliths analyzed in this study can be observed in an outcrop in North-west Gran Canaria (Tamaraceite, Fig. 1). Although not at the depth of the ocean crust beneath the island, the uplifted Pliocene shallow-water sediments at Tamaraceite offer an analogue to xeno-pumice formation at depth. This may be used as a conceptual analogue for sedimentary xeno-pumice formation beneath Gran Canaria, because a number of features seen in this outcrop are likely applicable to the understanding of xeno-pumice formation at deeper levels within and beneath the island. At Tamaraceite a series of pillow basalts and hyaloclastites of Pliocene (Roque Nublo) age is exposed, which is partly underlain by silt-marl-type sediment (Fig. 10; Perez-Torrado et al., 2014). Locally, the pillow basalts sank into the sediment and sedimentary rocks and so intruded the sedimentary materials in a sill-like fashion, thus interacting with the sediment to produce frothed up sedimentary lithologies that are analogous to xeno-pumice from El Hierro, Lanzarote, and from the highlands on Gran Canaria (cf. Rothe and Schmincke, 1968; Hansteen and Troll, 2003; Troll et al., 2012, 2015; Carracedo et al., 2015; Zaczek et al., 2015). Indeed, where lava underlies sediment, we see structural disturbance of the sedimentary layers and an increased number of vesicles in both the sediments and the intruding basalts (Fig. 10B). In fact, the vesicles in the adjacent sediment wrap around the intruding lava in what looks like fluid/vesicle pathways that migrated from the intrusion into the sediment, diminishing in intensity away from the contacts (Fig. 10C). This vesiculation 'aureole' of frothing via heating can be up to several tens of cm in thickness and has likely initiated a process of gas/fluid transport through these heated sediments.

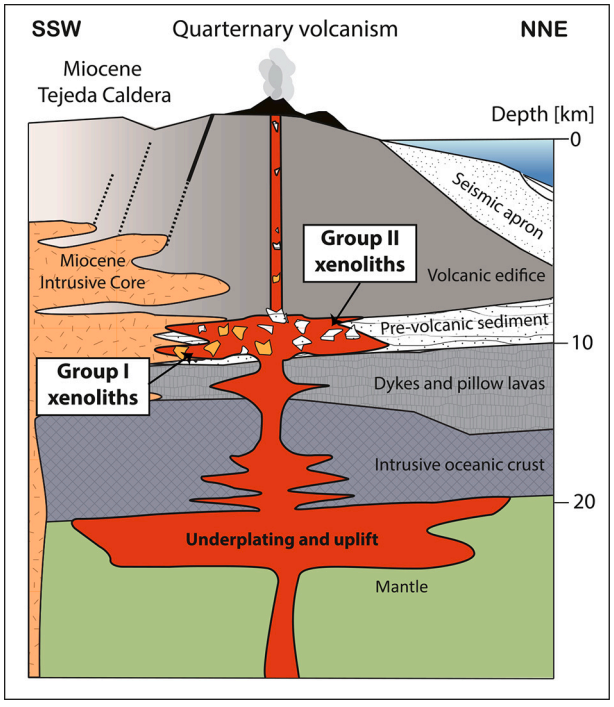

Fig. 11. Conceptual model of xeno-pumice formation in Quaternary volcanism on Gran Canaria, adapted from Ye et al. (1999), Hansteen and Troll (2003), and Aulinas et al. (2010b). During ascent melt pools and underplates the island edifice, causing uplift. Before the eruption, magma travels further through the subsurface, interacting with pre-existing bedrock (in this case sediments and intrusive rock) forming new magmatic conduits. Rapid degassing, assimilation and breakdown of wall-rock during partial melting immediately before eruption allows for the incorporation of the frothy felsic rock that erupts in the initial stages of eruption. When pathways from melt source to surface have been established, or when islands have matured, xeno-pumice production would decrease.

We suggest that the observed magma-sediment interaction features at Tamaraceite are also applicable to xeno-pumice formation at depth through propagation of magma through country rock in the sub-island sedimentary strata (Fig. 11). We realize that there is a difference in pressure between sub-island and near surface processes, but note that pore water contents in sediment can remain high even at several kilometers depth (Gluyas and Cade, 1997) and that H_2O contents will most probably exceed solubilities in high-silica magmas even at 10 km depth. The Tamaraceite outcrop can thus serve as a conceptual model for xeno-pumice formation at depth, although frothing may be less intense when the process occurs under several kilometers of overburden (see e.g., phase relations in Berg et al., 2016). Frothing would then certainly intensify during magma underplating and xenolith ascent while entrained in magma during conduit transport to the surface.

As exemplified in the Tamaraceite outcrop, magma pooling beneath and within the island edifice would allow for interaction between ascending melt and bedrock and formation of xeno-pumice at depth when stored magmas are emplaced into the low-density layers of the sedimentary horizon. Underplating and magma pooling at lithological boundaries is prevalent in several Canary Islands (e.g., La Palma; Klügel, 1998) and is likely to also occur at or in the sedimentary layers of the oceanic crust beneath Gran Canaria. Indeed, underplating beneath Gran Canaria was indicated by the measured uplift and subsequent tilt of Gran Canaria and especially in the NE section (Menéndez et al., 2008; Carracedo and Troll, 2016), and by seismic studies of the underlying mantle (Ye et al., 1999). We note that with progressive maturation of an ocean island, these pre-volcanic sedimentary deposits will be progressively replaced by magmatic intrusions, and we expect fewer sedimentary xenoliths in older volcanic islands. It can thus be expected that this type of magma-sediment interaction is not uncommon in most of the Canary Islands, especially in the younger islands, and in peripheral parts of more mature islands. Sedimentary xeno-pumice will thus likely occur in future eruptions in this part of Gran Canaria, as well as on the younger islands of the archipelago, while xeno-pumice of plutonic origin will probably be more common in central portions of mature islands (cf. Carracedo and Troll, 2016; Carracedo et al., 2022).

6. Conclusions

Our study of xeno-pumice on Gran Canaria yielded eight of the 14 analyzed xenoliths to be of pre-volcanic sedimentary origin, while the remaining six are of fresh to altered igneous origin representing previous volcanic episodes of the island. The sedimentary xenoliths appear to be from the pre-island oceanic crust and indicate magma transport through, interaction with, and possibly temporal magma storage within the sedimentary level of the ocean crust beneath the island (~10 km depth). In addition to magma storage at sub-island oceanic crustal levels, indicated by pre-island sedimentary rock fragments, transport of magma through the island's interior likely picked up various rocks of the 14 Ma to recent volcanic edifice of Gran Canaria. These remnants of both sedimentary and magmatic origin survived magmatic transport and were not fully assimilated by the rapidly ascending magmas. Lastly, the recently determined island tilt of Gran Canaria and relative uplift of the NE of the island may be the result of significant underplating, where ascending magma stagnates, interacts with, and replaces sub-island sedimentary strata and older igneous island rocks at depth.

Author statement

Conceptualization: VRT, FMD; Data Curation: SBJ, HG, CH, KZ; Formal Analysis: SBJ, VRT, HG, FMD, CH; Funding Acquistation: VRT, FMD, FMvdZ; Investigation: SBJ, VRT, HG, FMD, CH, KZ; Methodology: Not applicable (no development or design of new methods); Project Administration: VRT, FMD; Resources: VRT, HG, FMD, CH, JCC, FCM, KZ; Software: Not applicable (no software development); Supervision:

VRT, FMD; Validation: HG, CH; Visualization: SBJ, HG, FMD, SO; Writing - original draft: SBJ, VRT; Writing - review and editing: all authors SBJ, VRT, HG, FMD, CH, JCC, FCM, SO, KZ, FMvdZ.

Declaration of Competing Interest

The authors declare that they have no known competing financial interests or personal relationships that could have appeared to influence the work reported in this paper.

Data availability

Data will be made available on request.

Acknowledgments

We are grateful to F.J. Pérez-Torrado, A. Rodríguez-González, L.M. Schwarzkopf and P. Younger for help during field work and J. Majka for analytical support. Additional discussion with T.H. Hansteen, K. Hoernle, M.A. Longpré, J. Wolff, S. Wiesmaier, A, Klügel, B. Ellis, V. Soler, S. Berg, M. Aulinas, and C.J. Stillman are much appreciated. Reviews by U. Küppers and an anonymous referee are greatly appreciated. We thank the Swedish Science Foundation (VR), the Swedish Foundation for International Cooperation in Research and higher Education (STINT), Uppsala University (UU), and King Abdullah University of Science and Technology (KAUST) for support during this study. The University of Las Palmas de Gran Canaria (ULPGC) is thanked for logistical support during fieldwork.

Appendix A. Supplementary data

Supplementary data to this article can be found online at https://doi.org/10.1016/j.jvolgeores.2023.107857.

References

Allaz, J.M., Jercinovic, M.J., Williams, M.L., 2020. U-Th-Pb TOTAL dating of REE-phosphate by electron microprobe: Review and progress. In: IOP Conf. Series: Mater. Sci. Eng, 89. https://doi.org/10.1088/1757-899X/891/1/012001.

Anguita, F., Hernán, F., 1975. A propagating fracture model versus a hot spot origin for the Canary Islands. Earth Planet. Sci. Lett. 27, 11–19.

Anguita, F., Hernan, F., 2000. The Canary Islands origin: a unifying model. J. Volcanol. Geotherm. Res. 103, 1–26.

Aparicio, A., Bustillo, M.A., Garcia, R., Arana, V., 2006. Metasedimentary xenoliths in the lavas of the Timanfaya eruption (1730–1736, Lanzarote, Canary Islands): metamorphism and contamination processes. Geol. Mag. 143, 181–193.

Aparicio, A., Tassinari, C.C.G., Garcia, R., Arana, V., 2010. Sr and Nd isotope composition of the metamorphic, sedimentary and ultramafic xenoliths of Lanzarote (Canary Islands): Implications for magma sources. J. Volcanol. Geotherm. Res. 189, 143–150.

Araña, V., Ibarrola, E., 1973. Rhyolitic pumice in the basaltic pyroclasts from the 1971 eruption of Teneguía volcano, Canary Islands. Lithos 6, 273–278.

Aulinas, M., Gimeno, D., Fernández-Turiel, J.L., Font, L., Pérez-Torrado, F.J., Rodríguez-González, A., Nowell, G.M., 2010a. Small-scale mantle heterogeneity on the source of the Gran Canaria (Canary Islands) Pliocene-Quaternary magmas. Lithos 119, 377–392.

Aulinas, M., Gimeno, D., Fernandez-Turiel, J.L., Perez-Torrado, F.J., Rodriguez-Gonzalez, A., Gasperini, D., 2010b. The Plio-Quaternary magmatic feeding system beneath Gran Canaria (Canary Islands, Spain): constraints from thermobarometric studies. J. Geol. Soc. 67, 785–801.

Barker, A.K., Troll, V.R., Carracedo, J.C., Nicholls, P., 2015. The magma plumbing system for the 1971 Teneguía eruption on La Palma, Canary Islands. Contrib. Mineral. Petrol. 170, 54.

Berg, S.E., Troll, V.R., Deegan, F.M., Burchardt, S., Krumbholz, M., Mancini, L., Polacci, M., Carracedo, J.C., Soler, V., Arzilli, F., Brun, F., 2016. Heterogeneous vesiculation of 2011 El Hierro xeno-pumice revealed by X-ray computed microtomography. Bull. Volcanol. 78, 85.

Berg, S., Troll, V., Harris, C., Deegan, F., Riishuus, M., Burchardt, S., Krumbholz, M., 2018. Exceptionally high whole-rock δ18O values in intra-caldera rhyolites from Northeast Iceland. Mineral. Mag. 82, 1147–1168.

Bindeman, I., 2008. Oxygen Isotopes in Mantle and Crustal Magmas as Revealed by Single Crystal Analysis. Rev. Mineral. Geochem. 69, 445–478.

Bindeman, I.N., Deegan, F.M., Troll, V.R., Thordarson, T., Höskuldsson, Á., Moreland, W. M., Zorn, E.U., Shevchenko, A.V., Walter, T.R., 2022. Diverse mantle components with invariant oxygen isotopes in the 2021 Fagradalsfjall eruption, Iceland. Nat. Commun. 13 https://doi.org/10.1038/s41467-022-31348-7.

Carracedo, J.C., Troll, V.R., 2016. The Geology of the Canary Islands. Elsevier, p. 636.

Carracedo, J.C., Troll, V.R., 2021. North-East Atlantic Islands: the Macronesian Archipelagos. In: Alderton, D., Elias, S.A. (Eds.), Encyclopedia of Geology, Second edition. Academic Press, pp. 674–699.

Carracedo, J.C., Day, S.J., Guillou, H., Rodriguez Badiola, H., Canas, J.A., Pérez Torrado, F.J., 1998. Hotspot volcanism close to a passive continental margin: the Canary Islands. Geol. Mag. 135, 591–604.

Carracedo, J.C., Troll, V.R., Zaczek, K., Rodríguez-González, A., Soler, V., Deegan, F.M., 2015. The 2011–2012 submarine eruption off El Hierro, Canary Islands: New lessons in oceanic island growth and volcanic crisis management. Earth Sci. Rev. 150, 168–200.

Carracedo, J.C., Troll, V.R., Day, J.M., Geiger, H., Aulinas, M., Soler, V., Deegan, F.M., Perez-Torrado, F.J., Gisbert, G., Gazel, E., Rodriguez-Gonzalez, A., Albert, H., 2022. The 2021 eruption of the Cumbre Vieja Volcanic Ridge on La Palma, Canary Islands. Geol. Today 38, 94–107.

Collier, J.S., Watts, A.B., 2001. Lithospheric response to volcanic loading by the Canary Islands: Constraints from seismic reflection data in their flexural moat. Geophys. J. Int. 147, 660–676.

Cooper, K.M., Eiler, J.M., Sims, K.W.W., Langmuir, C.H., 2009. Distribution of recycled crust within the upper mantle: Insights from the oxygen isotope composition of MORB from the Australian-Antractic Discordance. Geochem. Geophys. Geosyst. 10 https://doi.org/10.1029/2009GC002728.

Cousens, B.L., Spera, F.J., Tilton, G.R., 1990. Isotopic patterns in silicic ignimbrites and lava flows of the Mogan and the lower Fataga Formations, Gran Canaria, Canary Islands: temporal changes in mantle source composition. Earth Planet. Sci. Lett. 96, 319–335.

Day, J.M.D., Troll, V.R., Aulinas, M., Deegan, F.M., Geiger, H., Carracedo, J.C., Gisbert, G., Perez-Torrado, F.J., 2022. Mantle source characteristics and magmatic processes during the 2021 La Palma eruption. Earth Planet. Sci. Lett. 597, 117793. https://doi.org/10.1016/j.epsl.2022.117793.

Deegan, F.M., Troll, V.R., Barker, A.K., Harris, C., Chadwick, J.P., Carracedo, J.C., Delcamp, A., 2012. Crustal versus source processes recorded in dykes from the Northeast volcanic rift zone of Tenerife, Canary Islands. Chem. Geol. 334, 324–344.

Donoghue, E., Troll, V.R., Harris, C., O'Halloran, A., Walter, T.R., Pèrez Torrado, F.J., 2008. Low- temperature hydrothermal alteration of intra-caldera tuffs, Miocene Tejeda caldera, Gran Canaria, Canary Islands. J. Volcanol. Geotherm. Res. 176, 551–564.

Del Moro, S., Di Roberto, A., Meletlidis, S., Pompilio, M., Bertagnini, A., Agostini, S., Ridolfi, F., Renzulli, A., 2015. Xenopumice erupted on 15 October 2011 offshore of El Hierro (Canary Islands): a subvolcanic snapshot of magmatic, hydrothermal and pyrometamorphic processes. Bull. Volcanol. 77, 53. https://doi.org/10.1007/s00445-015-0940-0.

Donoghue, E., Troll, V.R., Harris, C., 2010. Fluid-Rock Interaction in the Miocene, Post-Caldera,Tejeda Intrusive Complex,Gran Canaria (Canary Islands): Insights from Mineralogy, and O- and H-Isotope Geochemistry. J. Petrol. 51, 2149–2176.

Fagereng, A., Harris, C., La Grange, M., Stevens, G., 2008. Stable isotope study of the Archaean rocks of the Vredefort impact structure, central Kaapvaal Craton, South Africa. Contrib. Mineral. Petrol. 155, 63–78.

Gardner, M., Troll, V.R., Gamble, J., Gertisser, R., Hart, G., Ellam, R., Harris, C., Wolff, J., 2013. Crustal differentiation processes at Krakatau volcano, Indonesia. J. Petrol. 54, 149–182.

Gee, M.J.R., Watts, A.B., Masson, D.G., Mitchell, N.C., 2001. Landslides and the evolution of El Hierro in the Canary Islands. Mar. Geol. 177, 271–293.

Geiger, H., Mattsson, T., Deegan, F.M., Troll, V.R., Burchardt, S., Gudmundsson, Ó., Tryggvason, A., Krumbholz, M., Harris, C., 2016. Magma plumbing for the 2014–2015 Holuhraun eruption, Iceland. Geochem. Geophys. Geosyst. G3 (17), 2953–2968.

Glaccum, R.A., Prospero, J.M., 1980. Saharan aerosols over the tropical North Atlantic—Mineralogy. Mar. Geol. 37, 295–321.

Gluyas, J., Cade, C.A., 1997. Prediction of porosity in compacted sands. In: Kupecz, J.A., Gluyas, J., Bloch, S. (Eds.), Reservoir Quality Prediction in Sandstones and Carbonates, 69. AAPG Mem, pp. 19–28.

González, P.J., Samsonov, V.S., Pepe, S., Tiampo, K.F., Tizzani, P., Casu, F., Fernández, J., Camacho, A.G., Sansosti, E., 2013. Magma storage and migration associated with the 2011–2012 El Hierro eruption: Implications for crustal magmatic systems at oceanic island volcanoes. J. Geophys. Res. 118, 4361–4377.

Graettinger, A., Bennis, K., Brand, B., Reynolds, E., Nolan, J., 2020. Basaltic phreatomagmatic fissure at 71 Gulch Part 2: unusual pyroclasts from sediment magma mingling and melting. Bull. Volcanol. 82 https://doi.org/10.1007/s00445-020-01417-0.

Hansteen, T.H., Troll, V.R., 2003. Oxygen isotope composition of xenoliths from the oceanic crust and volcanic edifice beneath Gran Canaria (Canary Islands): consequences for crustal contamination of ascending magmas. Chem. Geol. 193, 181–193.

Hoernle, K., 1998. Geochemistry of Jurassic oceanic crust beneathGran Canaria (Canary Islands): implications for crustal recy-cling and assimilation. J. Petrol. 39, 859–880.

Hoernle, K., Schmincke, H.D., 1993. The role of partial melting in the IS-Ma geochemical evolution of Gran Canaria: a blob model for the Canary hotspot. 1. Petrol. 34, 599–626.

Hunt, J.E., Jarvis, I., 2017. Prodigious submarine landslides during the inception and early growth of volcanic islands. Nat. Commun. 8, 2061.

Jolis, E.M., Troll, V.R., Harris, C., Freda, C., Gaeta, M., Orsi, G., Siebe, C., 2015. Skarn xenolith record crustal CO2 liberation during Pompeii and Pollena eruptions, Vesuvius volcanic system, central Italy. Chem. Geol. 415, 17–36.

King, S.D., Ritsema, J., 2000. African hot spot volcanism: small-scale convection in the upper mantle beneath cratons. Science 290, 1137–1140.
Klügel, A., 1998. Reactions between mantle xenoliths and host magma beneath La Palma (Canary Islands): constraints on magma ascent rates and crustal reservoirs. Contrib. Mineral. Petrol. 131, 237–257.
Krastel, S., Schmincke, H.U., 2002. Crustal structure of northern Gran Canaria, Canary Islands, deduced from active seismic tomography. J. Volcanol. Geotherm. Res. 115 (1–2), 153–177.
Le Bas, M.J., Le Maitre, R.W., Streckeisen, A., Zanettin, B., 1986. A Chemical Classification of Volcanic Rocks Based on the Total Alkali-Silica Diagram. J. Petrol. 27, 745–750. https://doi.org/10.1093/petrology/27.3.745.
Lofgren, G., 1974. An experimental study of plagioclase crystal morphology: Isothermal crystallization. Am. J. Sci. 274, 243–273.
McDougall, I., Schmincke, H.U., 1976. Geochronology of Gran Canaria, Canary Islands: Age of Shield Building Volcanism and Other Magmatic Phases. Bull. Volcanol. 40.
Meletlidis, S., Di Roberto, A., Pompilio, M., Bertagnini, A., Iribarren, I., Felpeto, A., Torres, P.A., D'Oriano, C., 2012. Xenopumices from the 2011–2012 submarine eruption of El Hierro (Canary Islands, Spain): Constraints on the plumbing system and magma ascent. Geophys. Res. Lett. 39, L17302.
Menéndez, I., Silva, P.G., Martín-Betancor, M., José Pérez-Torrado, F., Guillou, H., Scaillet, S., 2008. Fluvial dissection, isostatic uplift, and geomorphological evolution of volcanic islands (Gran Canaria, Canary Islands, Spain). Geomorphology 102, 89–203.
Montel, J.-M., Foret, S., Veschambre, M., Nicollet, C., Provost, A., 1996. Electron microprobe dating of monazite. Chem. Geol. 131, 37–53.
Montelli, R., Nolet, G., Dahlen, F.A., Masters, G., Engdahl, E.R., Hung, S.H., 2004. Finite-Frequency Tomography reveals a Variety of Plumes in the Mantle. Science 303, 338–343.
Morgan, W.J., 1971. Convection Plumes in the lower Mantle. Nature 230.
Neumann, E.R., Wulff-Pedersen, E., Pearson, N.J., Spencer, E.A., 2002. Mantle xenoliths from Tenerife (Canary Islands): evidence for reactions between mantle peridotites and silicic carbonatite melts inducing ca metasomatism. J. Petrol. 43, 825–857.
Pérez-Torrado, F.F., Carracedo, J.C., Mangas, J., 1995. Geochronology and stratigraphy of the Roque Nublo Cycle, Gran Canaria, Canary Islands. J. Geol. Soc. 152 (5), 807–818.
Perez-Torrado, F.J., Gimeno, D., Aulinas, M., Cabrera, M.C., Guillou, G., Rodriguez-Gonzalez, A., Gisbert, G., Fernandez-Turiel, J.L., 2014. Polygonal feeder tubes filled with hydroclasts: a new volcanic lithofacies marking shoreline subaerial–submarine transition. J. Geol. Soc. 172, 29–43.
Ranero, C.R., Torne, M., Banda, E., 1995. Gravity and multichannel seismic reflection constraints on the lithospheric structure of the Canary Swell. Mar. Geophys. Res. 17, 519–534.
Rodriguez-Gonzalez, A., Fernandez-Turiel, J.L., Perez-Torrado, F.J., Hansen, A., Aulinas, M., Carracedo, J.C., Gimeno, D., Guillou, H., Paris, R., Paterne, M., 2009. The Holocene volcanic history of Gran Canaria Island: implications for volcanic hazards. J. Quat. Sci. 24, 697–709.
Rodriguez-Gonzalez, A., Perez-Torrado, F.J., Fernandez-Turiel, J.L., Aulinas, M., Paris, R., Moreno-Medina, C., 2018. The Holocene volcanism of Gran Canaria (Canary Islands, Spain). J. Maps 14, 620–829. https://doi.org/10.1080/17445647.2018.1526717.
Rodriguez-Losada, J.A., Eff-Darwich, A., Hernandez, L.E., Viñas, R., Pérez, N., Hernandez, P., Melian, G., Martínez-Frias, J., Romero-Ruiz, C.M., Coello-Bravo, J.J., 2015. Petrological and geochemical highlights in the floating fragments of the October 2011 submarine eruption offshore El Hierro (Canary Islands): Relevance of submarine hydrothermal processes. J. Afr. Earth Sci. 102, 41–49.
Rothe, P., Schmincke, H.U., 1968. Contrasting origins of the eastern and western islands of the Canarian Archipelago. Nature 218, 1152–1154.
Savin, S.M., Epstein, S., 1970a. The oxygen and hydrogen isotope geochemistry of clay minerals. Geochim. Cosmochim. Acta 34, 25–42.
Savin, S.M., Epstein, S., 1970b. The oxygen and hydrogen isotope geochemistry of ocean sediments and shales. Geochim. Cosmochim. Acta 34, 43–63.
Schipper, C.I., Rickard, W.D.A., Reddy, S.M., Saxey, D.W., Castro, J.M., Fougerouse, D., Quadir, Z., Conway, C., Prior, D.J., Lilly, K., 2020. Volcanic SiO2-cristobalite: A natural product of chemical vapor deposition. Am. Mineral. 105, 510–524.
Schmincke, H.U., 1982. Volcanic and chemical evolution of the Canary Islands. In: Von Rad, U., Hinz, K., Sarnthein, M., Seibold, E. (Eds.), Geology of the Northwest African Margin. Springer, Berlin, pp. 273–306.
Schmincke, H.U., Segschneider, B., 1998. Shallow submarine to emergent basaltic shield volcanism of Gran Canaria: evidence from drilling into the volcanic apron. In: Published in: Proceedings of Ocean Drilling Program, Scientific Results, 157, pp. 141–181.
Schmincke, H.U., Sumita, M., 1998. Volcanic Evolution of Gran Canaria reconstructed from apron sediments: synthesis of VICAP project drilling. In: Published in: Proceedings of the Ocean Drilling Program, Scientific Result, 157, pp. 443–469.
Schmincke, H.U., Sumita, M., 2010. Geological Evolution of the Canary Islands: A Young Volcanic Archipelago Adjacent to the Old African Continent. Göerres-Verlag, Germany, pp. 1–194.
Schmincke, H.U., Klügel, A., Hansteen, T.H., Hoernle, K., van den Bogaard, P., 1998. Samples from the Jurassic Ocean crust beneath Gran Canaria, La Palma and Lanzarote (Canary Islands). Earth Planet. Sci. Lett. 163 (1–4), 343–360.
Sigmarsson, O., Laporte, D., Carpentier, M., Devouard, B., Devidal, J.L., Marti, J., 2013. Formation of U-depleted rhyolite from a basanite at El Hierro, Canary Islands. Contrib. Mineral. Petrol. 165, 601–622.
Taylor, H.P., 1968. The oxygen isotope geochemistry of igneous rocks. Contrib. Mineral. Petrol. 19, 1–71. https://doi.org/10.1007/BF00371729.
Thirlwall, M.F., Jenkins, C., Vroon, P.Z., Mattey, D.P., 1997. Crustal interaction during construction of ocean islands: Pb– Sr–Nd–O isotope geochemistry of the shield basalts of Gran Canaria, Canary Islands. Chem. Geol. 135, 233–262.
Troll, V.R., Schmincke, H.U., 2002. Magma mixing and crustal recycling in ternary feldspar from compositionally zoned peralkaline ignimbrite 'A', Gran Canaria, Canary Islands. J. Petrol. 43, 243–270.
Troll, V.R., Klügel, A., Deegan, F.M., Carracedo, J.C., Wiesmaier, S., Kueppers, U., Dahren, B., Blythe, L.S., Hansteen, T.H., Freda, C., Budd, D.A., Jolis, E.M., Jonsson, E., Meade, F.C., Harris, C., Berg, S.E., Mancini, L., Polacci, M., Pedroza, K., 2012. Floating stones off El Hierro, Canary Islands: xenoliths of pre-island sedimentary origin in the early products of the October 2011 eruption. Solid Earth 3, 97–110.
Troll, V.R., Deegan, F.M., Burchardt, S., Zaczek, K., Carracedo, J.C., Meade, F.C., Soler, V., Cachao, M., Ferreira, J., Barker, A.K., 2015. Nannofossils: the smoking gun for the Canarian hotspot. Geol. Today 31, 137–145.
Troll, V.R., Carracedo, J.C., Gilg, H.A., 2022. African sandstorms, blood rain and continental mineral delivery to the Canary Islands. Geol. Today 38, 218–229.
van den Bogaard, P., Schmincke, H.U., 1998. Chronostratigraphy of Gran Canaria. In: Published in: Proceedings of the Ocean Drilling Program: Scientific Results, 157 (Chapter 11), 147-140.
Vennemann, T.W., Smith, H.S., 1990. The rate and temperature of reaction of CIF3 with silicate minerals, and their relevance to oxygen isotope analysis. Chem. Geol. 86, 83–88.
Ye, S., Canales, J.P., Rihm, R., Danobeitia, J.J., Gallart, J., 1999. A crustal transect through the northern and northeastern part of the volcanic edifice of Gran Canaria, Canary Islands. Geodynamics 28, 3–26.
Zaczek, K., Troll, V.R., Cachao, M., Ferreira, J., Deegan, F.M., Juan, C., Soler, V., Meade, F.C., Burchardt, S., 2015. Nannofossils in 2011 El Hierro eruptive products reinstate plume model for Canary Islands. Sci. Rep. 5, 7945.